FAR-ULTRAVIOLET CONTINUUM OF G-TYPE STARS: A SIGNATURE OF THE TEMPERATURE MINIMUM REGION[1]

M. FRANCHINI AND C. MOROSSI

Osservatorio Astronomico di Trieste, Via G. B. Tiepolo, 11, I–34131 Trieste, Italy; franchini@oat.ts.astro.it, morossi@oat.ts.astro.it

M. L. MALAGNINI

Dipartimento di Astronomia, Università degli Studi di Trieste, Via G. B. Tiepolo, 11, I–34131 Trieste, Italy; malagnini@daut.univ.trieste.it

ABSTRACT

The main results of a program of systematic comparison between observed and computed UV spectral energy distributions of field G-type stars are illustrated. We constructed the UV observed energy distributions for 53 G stars, starting from the *IUE* Uniform Low Dispersion Archive (ULDA) and computed the corresponding theoretical fluxes by using the atmospheric parameters from the Catalogue of [Fe/H] Determinations (1996 edition) and a Kurucz grid of model fluxes. From the comparison between observations and classical models, a UV excess shortward of 2000 Å is evident for all the program stars. The UV continuum in the region 1600–2000 Å can be described by synthetic fluxes computed from semiempirical models based on the temperature minimum concept. Values for the T_{min}/T_{eff} ratio on the order of 0.80 are suitable for the interpretation of the observed fluxes. The residual discrepancies shortward of 1600 Å are suggested to be effects of the chromosphere, on the basis of a comparison with the Maltby et al. semiempirical model of the Sun.

Subject headings: stars: atmospheres — stars: chromospheres — stars: late-type — ultraviolet: stars

1. INTRODUCTION

Analysis of the spectral energy distributions (SEDs) of cool stars has received a strong incentive in recent years from the availability of improved models and extended observational facilities from space. In particular, great attention has been paid to the (far) ultraviolet region, accessible through *IUE*, where chromospheric activity of late-type stars shows up with prominent features. More recently, both joint observations in X-ray and UV and new data from instruments such as *Hubble Space Telescope* GHRS greatly improved the understanding of the chromospheric properties of F–K stars. While most papers on this subject are based on the analysis of emission lines (see, e.g., the review by Haisch & Schmitt 1996 and references therein), the present paper focuses on the study of the UV continuum itself as a diagnostic of the presence of nonradiative heating in the outer atmosphere, and in particular of the temperature minimum region. In this context, we present the results of analyses in the UV of a representative sample of G-type stars.

In the framework of a systematic comparison between observed and computed spectral energy distributions of cool stars, we previously analyzed a sample of K-type stars in the *IUE* ultraviolet region (Morossi et al. 1993). The main result of the analysis of the K stars was the failure of theoretical classical models in predicting the near-UV (2200 Å < λ < 3000 Å) SEDs of stars showing, even at low resolution, chromospheric features such as the Mg II resonance doublet in emission. Similar results were obtained from an analysis of a limited sample of G8 giants of Population II (Malagnini, Morossi, & Franchini 1994). Morossi et al. (1993) presented semiempirical models (hereafter T_{min}

models) based on a modified temperature structure with respect to classical models, obtained by taking into account the presence in the upper photosphere of a temperature minimum region. The fluxes computed starting from this new set of models provided a fairly good description of the observations in the near-UV of late G and K stars. In this paper, we will extend the analysis to earlier spectral type stars and to shorter wavelength regions. In particular, we will show where and how the overall UV SEDs show signatures of the presence of outer-atmosphere structures not included in the temperature structure of classical models.

In § 2 the program stars and the observational and theoretical data sets are illustrated, in § 3 the observations are analyzed and compared with the predictions of classical and T_{min} models, and in § 4 conclusions are presented.

2. THE DATA SETS

2.1. *The Program Stars*

The starting working set is given by the subset of the G-type field stars listed in Cayrel et al. (1997, hereafter 1996 Catalog), selected according to the following requirements:

1. Availability of at least one complete set of atmospheric parameters, namely, effective temperature (T_{eff}), surface gravity (log g), and chemical composition ([Fe/H]).
2. Availability of at least one *IUE*/SWP good-quality spectrum in the ULDA database.

We extracted from the ULDA archive (version 4.0), which contains the low-resolution *IUE* spectra obtained up to 1991 December 31, all the SWP-calibrated spectra referring to the whole set of field G-type stars listed in the 1996 Catalog.[2] The spectra classified as "dubious" and/or over or underexposed were rejected, and the subset of SWP good-quality spectra taken with the large aperture of the

[2] Checks on a sample of spectra using the *IUE* final archive, which is currently being produced, showed no significant differences in the calibrated spectra.

TABLE 1

PROGRAM STARS, ATMOSPHERIC STELLAR PARAMETERS, AND R-VALUES

HD No.	Spectral Class	Object Type	V	$B-V$	N_{SW}	N_{LW}	T_{eff}	log g	[Fe/H]	R
2151	G2IV	V	2.80	0.62	3		5860	4.15	−0.10	0.80
							5860	4.20	−0.20	0.79
							5860	4.30	−0.17	0.79
							5860	4.00	0.00	0.80
							5727	3.75	−0.10	0.82
							5727	4.40	−0.23	0.82
							5727	3.80	−0.28	0.82
							5727	3.80	−0.31	0.82
6582	G5Vb	SB	5.12	0.69	2	1	5336	4.39	−0.86	0.82
							5305	4.61	−0.71	0.83
							5091	4.20	−0.57	0.86
							5196	4.50	−0.55	0.85
							5305	4.50	−0.90	0.83
9270	G7IIa	V	3.61	0.98	1		4910	2.80	−0.14	
10700	G8V	PM	3.50	0.72	6	2	5250	4.65	−0.46	0.83
							5305	4.32	−0.66	0.81
							5305	4.33	−0.49	0.81
							5362	4.59	−0.34	0.81
							4990	4.50	−0.56	0.86
							5250	4.50	−0.58	0.82
							5143	3.60	−0.60	0.84
13421	G0IV		5.60	0.59	1		6165	4.00	0.36	0.80
20630	G5Vvar	V	4.83	0.68	10		5667	4.29	−0.01	0.85
							5663	4.45	0.08	0.85
							5600	4.50	0.04	0.85
							5663	4.40	−0.01	0.85
20766	G2.5V	PM	5.54	0.64	1		5860	4.75	0.10	0.82
							5666	4.36	−0.37	0.83
							5860	4.50	−0.20	0.80
							5478	3.80	−0.10	0.87
							5478	3.80	−0.35	0.86
20794	G8V	PM	4.27	0.71	26	1	5663	4.50	0.00	0.78
							5498	4.25	−0.48	0.80
							5362	4.40	−0.51	0.82
							5362	4.40	−0.34	0.82
							5305	4.20	−0.44	0.83
							5362	4.17	−0.54	0.81
20807	G1V	PM	5.24	0.60	1		5889	4.41	−0.23	0.81
							6072	4.70	0.10	0.79
							5856	4.40	−0.38	0.80
							6000	4.50	−0.20	0.79
							5600	4.50	−0.42	0.85
							5600	4.51	−0.32	0.85
							5727	4.00	−0.04	0.84
							5640	3.94	−0.07	0.85
28305	G9.5III	**	3.50	1.04	4		4820	2.77	0.04	0.76:
							4800	2.20	−0.04	0.76:
30495	G3V	PM	5.50	0.64	2		6000	4.50	0.10	0.81
							5829	4.30	−0.13	0.83
31910	G1Ib II	**	4.03	0.92	1	1	5400	1.50	−0.25	0.87
34411	G1.5IV-V	PM	4.70	0.64	1	1	5860	4.30	0.06	0.81
							5889	4.12	−0.03	0.80
							5860	4.16	−0.08	0.81
							5845	4.22	0.10	0.81
							5860	4.10	0.30	0.82
							5860	4.11	0.35	0.82
36079	G5II	**	2.84	0.82	2		5225	2.10	0.05	0.81
							5170	2.27	−0.44	0.81
39587	G0V	PM	4.41	0.59	3	2	6000	4.44	−0.12	0.82
							5953	4.46	−0.03	0.83
							5900	4.21	−0.05	0.84
							5929	4.50	−0.05	0.83
44594	G3V	PM	6.61	0.65	1	2	5793	4.43	0.13	0.81
52973	G0Ibvar	Ce	3.79	0.79	9	14	5727	1.50	0.49	0.77
							5727	1.50	0.21	0.77
							5727	1.90	0.33	0.77
65699	G8II		5.11	1.12	1		4846	1.50	−0.20	0.89
							4846	1.50	−0.09	0.89
72905	G1.5Vb		5.60	0.66	9	7	5793	4.40	−0.27	0.85
74772	G5III	**	4.07	0.87	1	1	5210	2.50	−0.03	0.82
77912	G8Iab:		4.56	1.04	1	1	5000	2.00	0.38	0.86
82210	G4III-IV	V	4.60	0.73	5		5305	3.58	−0.38	0.87

TABLE 1—*Continued*

HD No.	Spectral Class	Object Type	V	B−V	N_{SW}	N_{LW}	T_{eff}	log g	[Fe/H]	R
							5250	3.42	−0.34	0.88
82635	G8III	V	4.60	0.87	1		4960	3.00	−0.15	0.89
84737	G0.5Va	PM	5.10	0.61	1		5899	4.12	0.04	0.82
							5860	4.27	−0.04	0.82
85444	G6/G8III		4.12	0.92	2	1	5000	2.93	−0.14	0.87
95128	G1V	PM	5.10	0.56	1	2	5882	4.34	0.01	0.81
							5860	4.31	−0.02	0.81
101501	G8V	V	5.32	0.73	3		5538	4.69	0.03	0.83
							5478	4.60	−0.14	0.83
102365	G5V	PM	4.89	0.68	2	2	5569	4.34	−0.28	0.83
							5569	4.16	−0.42	0.83
							5419	4.10	−0.70	0.84
							5419	4.08	−0.48	0.85
109358	G0V	SB	4.26	0.59	1	1	6000	4.42	−0.03	0.81
							6000	4.50	0.00	0.81
							6000	4.50	0.05	0.81
							5879	4.52	−0.19	0.81
							5860	4.40	−0.19	0.82
							6000	4.50	0.07	0.81
							5860	4.35	0.08	0.83
109379	G5II	V	2.65	0.89	4		5170	2.10	−0.11	0.82
							5125	2.20	0.27	0.83
115383	G0Vs	PM	5.22	0.59	1	2	6021	4.15	0.10	0.85
							6072	4.20	0.04	0.84
							5929	4.44	0.10	0.86
							6018	4.21	0.08	0.85
115659	G8III	V	3.00	0.92	2		5080	2.90	−0.12	0.79:
							5025	2.60	0.06	0.80:
121370	G0IV	SB	2.68	0.58	1		6219	4.01	0.30	0.78
							6222	3.80	0.16	0.77
							6068	3.83	0.19	0.80
							6000	3.83	0.16	0.82
131117	G1V	PM	6.29	0.60	1		6001	4.09	0.13	0.83
135722	G8III	V	3.47	0.95	2	1	4830	2.93	−0.44	0.77
							4800	2.70	−0.50	0.78
							4800	2.00	−0.26	0.78
141714	G3.5III		4.63	0.80	1		5230	3.15	−0.32	0.87
144608	G6/G8III	V	4.32	0.84	2		5200	2.10	0.27	0.87
147675	G9III		3.89	0.91	1		5040	3.50	−0.05	0.86
148387	G8IIIb	V	2.74	0.91	2		5040	2.30	−0.07	0.77
							4940	3.10	−0.21	0.78
161797	G5IV	PM	3.41	0.76	2	1	5520	3.70	0.04	0.81
							5538	3.91	0.16	0.81
							5419	4.10	0.30	0.82
							5419	4.10	0.32	0.82
163993	G8III		3.70	0.94	3	1	5030	2.92	−0.10	0.83
							4990	2.50	0.27	0.84
166208	G8IIICN...		5.00	0.91	1		5075	2.65	0.14	0.87
							5000	2.76	−0.06	0.88
180711	G9III	**	3.07	1.00	1		4941	3.00	0.09	0.70:
							4820	2.98	−0.27	0.70:
							4893	2.10	0.00	0.70:
182572	G8IV...	V	5.16	0.77	2		5727	4.13	0.44	0.80
							5727	4.60	0.39	0.79
							5663	4.26	0.50	0.80
							5663	4.00	0.21	0.80
							5380	3.92	0.15	0.83
185758	G1II	**	4.37	0.78	1		5440	3.11	−0.15	0.86
185958	G8IIIa		4.37	1.05	1		4850	2.79	−0.03	0.80:
							4825	2.25	0.02	0.80:
186427	G3V	PM	6.20	0.66	3	17	5793	4.40	0.00	0.80
							5860	4.50	0.08	0.78
							5753	4.33	0.06	0.81
188512	G8IV	V	3.71	0.86	1		5478	1.30	0.20	0.76
							5250	3.79	−0.15	0.78
							5091	3.15	0.29	0.80
							5100	3.60	−0.30	0.79
190248	G7IV	V	3.56	0.76	4	1	5600	4.31	0.43	0.77
							5600	4.30	0.32	0.77
							5538	3.80	0.28	0.78
196755	G5IV+...	PM	5.05	0.72	1		5663	4.40	−0.05	0.81
							5520	3.42	−0.07	0.83
203387	G8III		4.28	0.90	1		5250	2.75	0.13	0.86

TABLE 1—*Continued*

HD No.	Spectral Class	Object Type	V	B−V	N_{SW}	N_{LW}	T_{eff}	log g	[Fe/H]	R
							5080	2.74	−0.23	0.88
216131......	G8III		3.48	0.93	1		5060	3.05	−0.16	0.77
							4950	2.50	−0.03	0.79
222574......	G2Ib/II	**	4.82	0.82	1		5478	1.80	0.05	0.85

spectrograph was extracted. The same procedure was applied to extract the corresponding LWR and/or LWP good-quality spectra. Then all the spectra of the same object were averaged, taking into account the different exposure times and discarding the data points flagged by bad quality marks. The average spectra have an accuracy on the order of ±10%, as a result of systematic uncertainties in the absolute flux calibration (up to ±5%) and camera(s) sensitivity degradation (up to ±5%) and temperature dependency (up to ±4.5%).

Eventually, we discarded, after visual inspection, a few spectra clearly inconsistent with the spectral classification of the star and the stars whose *IUE* spectra might be contaminated by contributions from companions.

We obtained a total of 53 stars, the data for which are reported in Table 1: spectral classification, object type, visual magnitude, B−V color index, and atmospheric parameters are from the 1996 Catalog; the numbers of SWP (N_{SW}) and of LWP/LWR (N_{LW}) images used to construct the mean SEDs are also reported.

2.2. *The Classical Model Fluxes*

The atmosphere models computed by R. L. Kurucz (1997, private communication) were assumed as classical LTE representations of the atmospheres of G-type stars. Thus, theoretical fluxes were computed for each of the 53 program stars starting from the Kurucz set of models and using the proper values for the atmospheric parameters (T_{eff}, log g, [M/H]). Unfortunately, in most cases more than one set of parameters is available in the 1996 Catalog (see Table 1), and the choice among the sets is not straightforward. The ranges of the parameters, referring to the total number of 150 sets, are 4800 K ≤ T_{eff} ≤ 6222 K, 1.30 dex ≤ log g ≤ 4.75 dex, and −0.90 dex ≤ [Fe/H] ≤ +0.50 dex; the spreads in the parameter values for the stars with more than one set of determinations reach at maximum ΔT_{eff} = 472 K (HD 20807), Δlog g = 2.49 dex (HD 188512), and Δ[Fe/H] = 0.59 dex (HD 188512). Therefore, for each star as many model fluxes (N_{mod}) as the number of available sets were derived from the Kurucz grid by interpolating linearly in the three-dimensional space (T_{eff}, log g, [M/H]). We should notice that the use of the theoretical [M/H] in place of the observed [Fe/H] implies that all metal abundances are scaled by the same factor with respect to the solar ones.

In order to compare theoretical predictions with observational data, the model fluxes were scaled to the observed visual magnitudes of the corresponding star.

2.3. T_{min} *Model Fluxes*

The temperature structure in classical models is characterized by a monotonic decrease toward the stellar surface, while in real stars a temperature minimum followed by a temperature rise is expected. As a first approximation to the real structure, we adopted a constant value for the tem-

perature outward of the expected minimum temperature location, and computed using ATLAS 9 (Kurucz 1993) three new grids of T_{min} model fluxes by selecting values of 0.70, 0.80, and 0.90 for the ratio between the minimum temperature and the effective temperature of the model, T_{min}/T_{eff}. For each star, N_{mod} T_{min} model fluxes were computed from each of the three new grids by interpolating linearly in the three-dimensional space (T_{eff}, log g, [M/H]).

3. ANALYSIS OF THE ULTRAVIOLET SPECTRAL ENERGY DISTRIBUTIONS

3.1. *Descattering*

It is well known that spurious light is present in the SWP range because of scattering along the dispersion of the gratings (Basri et al. 1985). To remove the spurious light from our spectra, we adopted the procedure of descattering proposed by Basri (1985), using as input spectrum the *IUE* observations, complemented longward of 3000 Å by classical model fluxes in order to mimic the visual flux distribution that is the origin of most of the scattered light. The descattering procedure was applied to the average spectra rather than to individual spectra in order to use higher S/N input data. For the same star, the use of different models, even T_{min}, did not introduce any significant difference in the resulting descattered spectrum. The descattered data referred to in the following discussion are derived using the model fluxes showing the lowest discrepancies with respect to LWP/LWR data or, when available, with respect to the fluxes derived from the *Astronomical Netherlands Satellite* (*ANS*) Ultraviolet Photometry Catalogue of Point Sources (Wesselius et al. 1982, hereafter *ANS* Catalog).

In order to illustrate the process, we use HD 131156 (G8 V), present in the initial working set and for which *HST*/GHRS archive data are available. Figure 1 shows the SWP spectrum of HD 131156 before and after descattering; as can be seen, the correction becomes important shortward
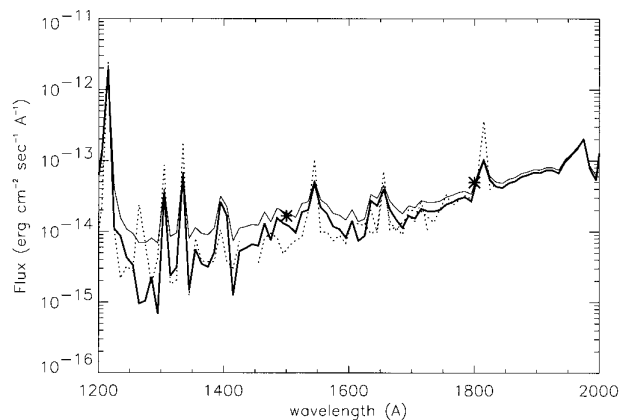

FIG. 1.—Flux distributions for HD 131156: *IUE* observations (*thin line*), *HST*/GHRS observations (*dotted line*), descattered fluxes (*thick line*), and *ANS* data (*asterisks*).

of 1800 Å. The good accuracy of the correction can be appreciated by comparing the descattered spectrum with the GHRS observations. The latter are free of mid-UV and visual scattered light, because of the detector blindness (Gessner, Carpenter, & Robinson 1994), and show a good agreement with the *IUE*-corrected data.

A further check on the reliability of the corrected spectra comes from comparison with the *ANS* observations. There are 27 stars in our sample that are also listed in the *ANS* Catalog, for which data in one or more of the five *ANS* bands are available. Only HD 2151 and HD 121370 have observed magnitudes in the 15W band, which is centered at 1549 Å, with bandpass of 149 Å. For these stars, Figure 2 shows the SWP and *ANS* data, together with the descattered spectra: it can be seen here that both the original and the descattered data are consistent with the *ANS* photometry in the 18 band, while at 15W the descattered data are significantly closer to the observed *ANS* value than the original *IUE* data.

Based on these direct checks for the stars HD 2151, HD 131156, and HD 121370, we are confident of the reliability of the descattering procedure for the whole set of stars that have quite similar spectral energy distributions.

In the following discussion we will always refer to the descattered fluxes.

3.2. Comparison with Classical Model Fluxes

The resulting spectra, referring to 53 bona fide individual G-type stars, were resampled at the same wavelength points and resolution as the model fluxes in the SWP wavelength range.
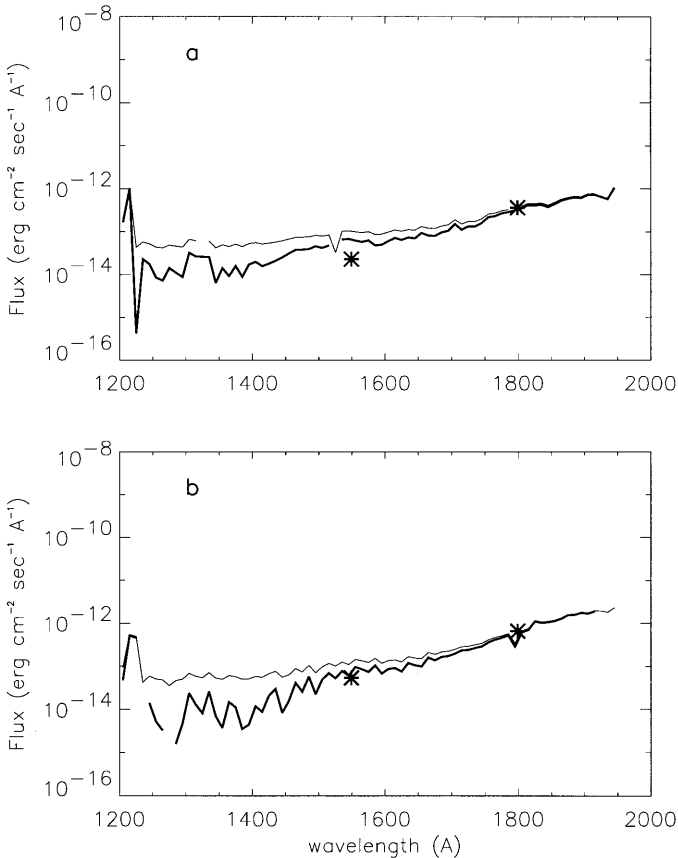
FIG. 2.—Flux distributions for (*a*) HD 2151 and (*b*) HD 121370: *IUE* observations (*thin line*), descattered fluxes (*thick line*), and *ANS* data (*asterisks*).
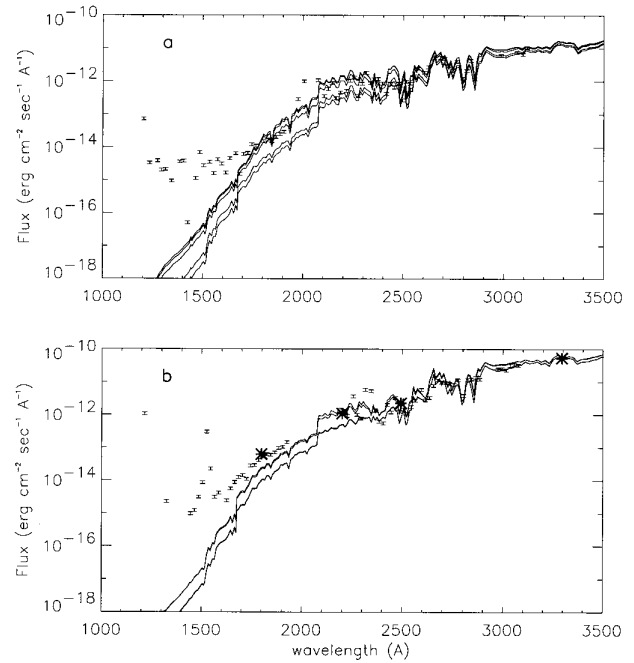
FIG. 3.—Flux distributions for (*a*) HD 6582 and (*b*) HD 161797: *IUE* descattered data are represented by $\pm 10\%$ error bars and *ANS* data by asterisks; classical model fluxes corresponding to different sets of atmospheric parameters are shown by solid lines.

The corrected absolute ultraviolet fluxes were plotted as a function of wavelength together with the classical model fluxes computed for the sets of atmospheric parameters available for each star. It may be worth noting that no dereddening was required, since for the nearby bright stars under study the $E(B-V)$ color excess values are negligible.

We find that the behavior of all the program stars is similar to that illustrated in Figure 3: the observed data shortward of about 2000 Å show a clear UV excess with respect to the synthetic fluxes. It is important to note that the discrepancy is orders of magnitude higher than the observational uncertainties (represented by $\pm 10\%$ error bars in the figures). While the UV excess is always present, irrespective of the particular choice of $T_{\rm eff}$, log g, and [M/H], a quantitative estimate of the discrepancy as a function of wavelength depends upon the adopted model.

A possible bias against the generalization of this UV excess phenomenon to all G-type stars may arise from the biased characteristics of the *IUE* database. In fact, the stellar activity, for example, could have been one of the key reasons for the observational proposals. In order to investigate the general relevance of our sample of stars, and therefore of the UV excess, we checked our data against the UV behavior of the unbiased collection of intrinsic *ANS* UV indexes from Kjærgaard et al. (1984). Starting from our *IUE* data, we computed a set of magnitudes (hereafter *IUE-ANS*) in the *ANS* passbands by applying the STScI (1995) SYNPHOT package.[3] These magnitudes, complemented with *ANS* magnitudes from the *ANS* Catalog (mainly in the 22 and 25 bands, when LW *IUE* spectra are not available), were used to compute *UV-V* indexes. Figure 4 shows that, apart from a very limited number of scattered points, the

---

[3] The consistency of the *IUE-ANS* magnitudes with the *ANS* magnitudes was successfully checked for the program stars present in the *ANS* Catalog.
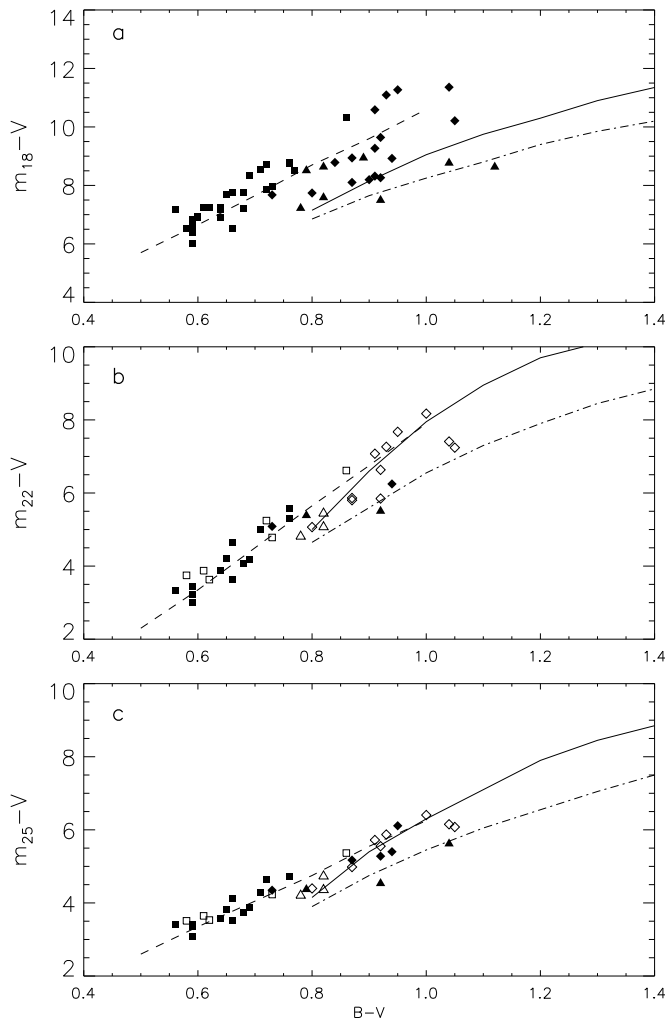
FIG. 4.—Color indexes (a) $m_{18} - V$, (b) $m_{22} - V$, and (c) $m_{25} - V$ vs. $B - V$, together with the sequences of intrinsic indexes from Kjærgaard et al. (1984). Whenever available, the indexes are computed by using *IUE-ANS* magnitudes (*filled symbols*); otherwise by using *ANS* magnitudes (*open symbols*). Different symbols are used for supergiants (*dash-dotted lines, triangles*), giants (*solid lines, diamonds*), and dwarfs (*dashed lines, squares*).
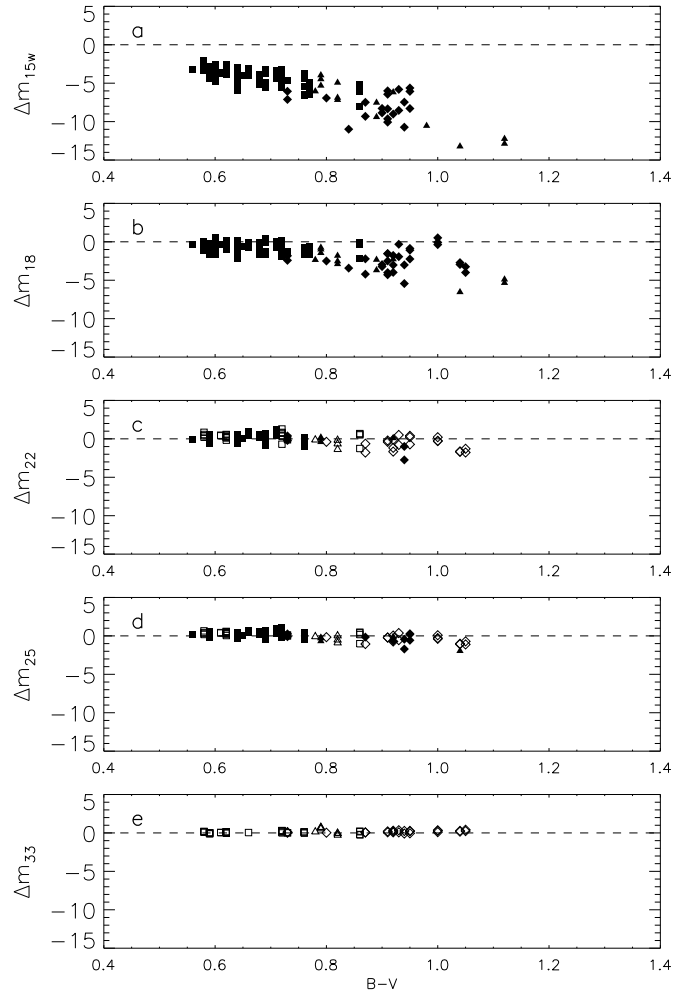

FIG. 5.—Differences (star-model) in the indexes (a) $m_{15W} - V$, (b) $m_{18} - V$, (c) $m_{22} - V$, (d) $m_{25} - V$, and (e) $m_{33} - V$ vs. $B - V$. Supergiants, giants, and dwarfs are represented by triangles, diamonds, and squares, respectively. The differences are computed by using *IUE-ANS* magnitudes (*filled symbols*) when available, or observed *ANS* (*open symbols*) otherwise.

values of the indexes pertaining to the program stars are fully consistent with the locations of the reference intrinsic indexes, thus permitting us to consider the sample of *IUE* observations under study unbiased, and to conclude that the divergence between observed and computed fluxes in the ultraviolet region is a general phenomenon for G-type stars.

The UV excesses of the data with respect to the models were computed using *ANS*, *IUE-ANS*, and synthetic indexes. As has already been pointed out, more than one model can be assigned to each star according to the 1996 Catalog; thus, more than one value for the synthetic colors can be computed for each object. Notwithstanding the multiplicity introduced by this fact, it is evident from Figure 5 that the UV excess is more pronounced in the 15W band than in the others. The differences between observed and computed colors are negligible and show no trend with luminosity class and/or $B - V$ in the 22, 25, and 33 bands. In the 15W and 18 bands, the differences are significant and increase with decreasing $B - V$. The UV excess is clearly present in the 15W band for all the stars, and there is no

clearly different behavior in different luminosity classes. The discrepancies between observations and predictions in the 15W and 18 bands are consistent with the findings by Edvardsson et al. (1993) for nearby field F and G disk stars (see their Fig. 3 and Table 5).

It must be stressed that most of the scatter among the points in Figures 5a and 5b is due to the use of more than one reference classical model for each star (see §§ 2.2 and 3.3). Unfortunately, this spurious scatter prevents us from investigating the effects, if any, of other hidden parameters, such as, for example, chemical composition and rotational velocity.

The UV excess may be due to a companion star, but known binary or multiple systems were dropped from the working set. Thus, the motivation related to binarity is unlikely for the program stars in general, even if the presence of a very dim companion responsible for at least a fraction of the UV excess cannot be completely ruled out.

On the other hand, the attribution of the UV excess to residual scattered light in the *IUE* data can be discarded, because of the good accuracy of the adopted descattering procedure (see § 3.1). Moreover, we recall that the UV

excess is already clearly present in the 18 *IUE-ANS* band, which is almost unaffected by spurious light and which is, in any case, confirmed by the behavior of the *ANS* data.

In conclusion, we consider the observed UV excess to be a clear signal of the presence of a chromosphere, as expected for active cool stars.

3.3. *Comparison with T_{min} Model Fluxes*

We used the T_{min} model fluxes to see whether the UV excess can be due to the presence of the temperature minimum region expected in the atmospheres of cool stars. The effect of such a region on the UV fluxes of K-type stars can be appreciated in Figure 2 of Morossi et al. (1993), where the fluxes computed as described in § 2.3 clearly provide a better match to the observations than do the classical model fluxes.

In fact, the T_{min} models mimic the effect of nonradiative heating in the upper photosphere. Morossi, Franchini, & Malagnini (1997) showed that increasing the model effective temperature moves the starting point of the predicted UV excess toward shorter wavelengths. Therefore, the deviations from classical model predictions, which happen shortward of 3000 Å for K stars, are expected to show up in the SWP wavelength region for G-type stars.

The ratio T_{min}/T_{eff}, as evaluated from high-resolution analyses of chromospheric emission lines, ranges from 0.71 (α Cen B, α Tau) to 0.94 (YZ CMi) (see, e.g., Kelch, Linsky, & Worden 1979 and references therein), being 0.7616 for the Sun (Maltby et al. 1986). Haisch & Basri (1985) have already shown that the 1600 Å $< \lambda < 2000$ Å region could be used to estimate the minimum temperature values in the atmospheres of solar-like stars. They analyzed a sample of 14 stars, and by using black body fitting in addition to classical models found T_{min}/T_{eff} from 0.78 up to about 0.90 for solar-like stars. A similar range was derived by Morossi et al. (1993) for a sample of G8–K5 stars.

The effect of different T_{min}/T_{eff} values on the predicted UV fluxes is illustrated in Figures 6 and 7 for HD 121370 and HD 6582, respectively. The flux distributions computed for three different $R = T_{min}/T_{eff}$ values, namely 0.70, 0.80,
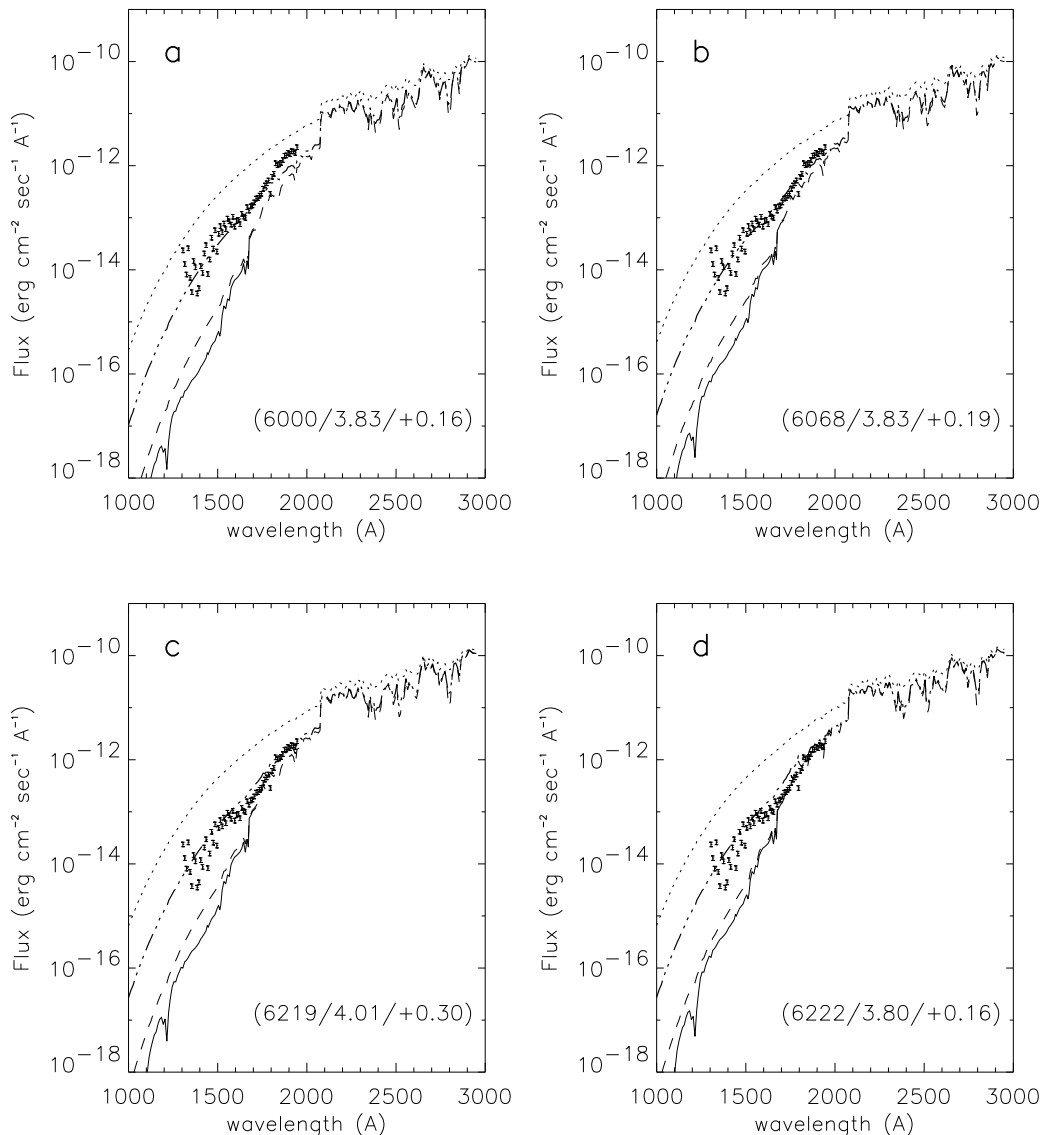

FIG. 6.—Observed flux distribution for HD 121379 ($\pm 10\%$ error bars) and T_{min} synthetic fluxes corresponding to $T_{min}/T_{eff} = 0.70$ (*dashed line*), 0.80 (*dash-dotted line*), and 0.90 (*dotted line*). The ultraviolet fluxes computed from the R. L. Kurucz (1997, private communication) classical model (*solid line*) are also plotted.
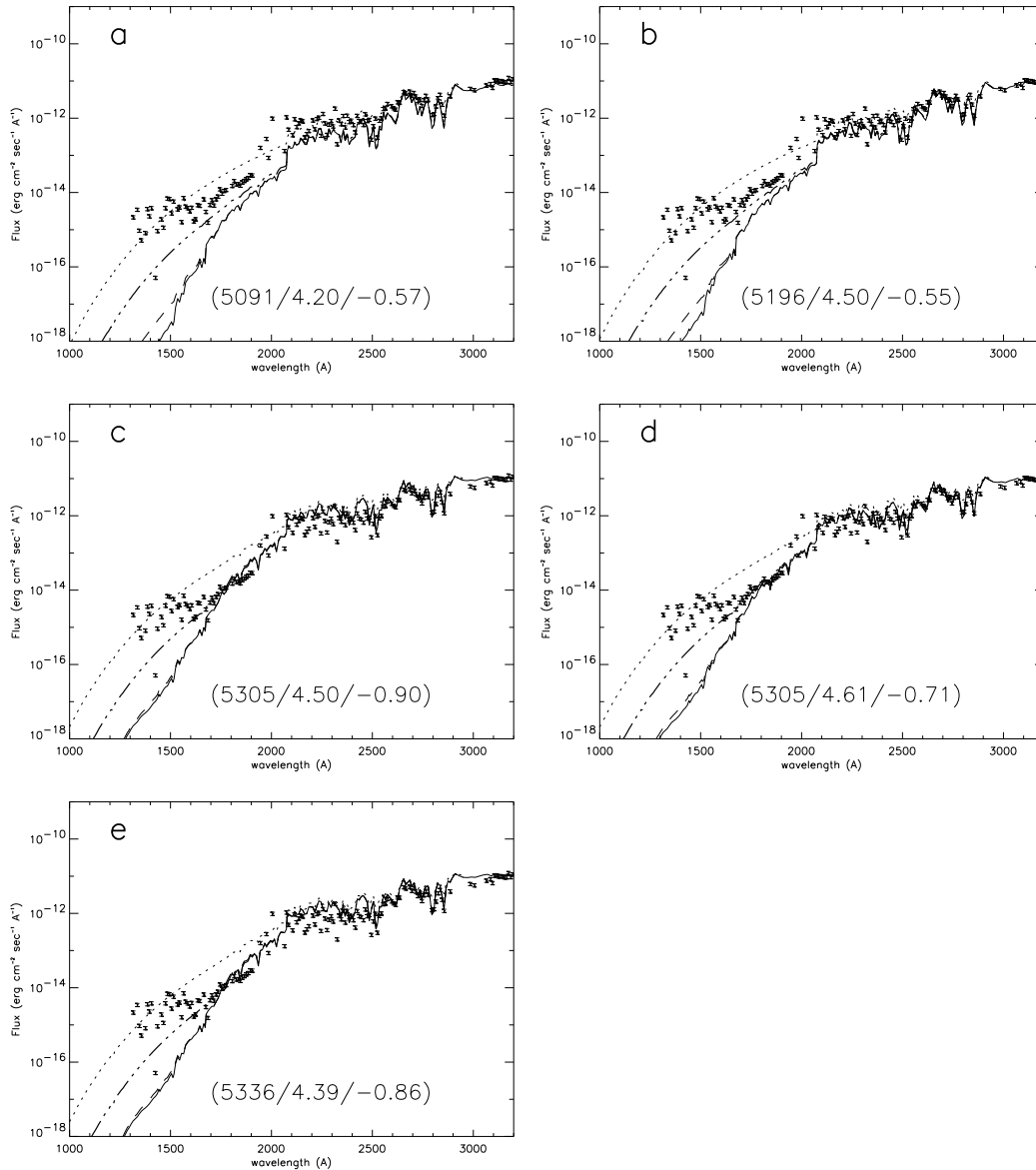
Fig. 7.—Same as Fig. 6, for HD 6582

and 0.90, are plotted after normalization at the visual magnitude of each star. It appears that the T_{min} model fluxes do not show the strong absorption features predicted by the classical models, and that the predicted UV flux shortward of about 2000 Å increases with increasing T_{min}/T_{eff}.

In general, for all the program stars, the fluxes predicted by T_{min} models with R in the 0.70–0.90 range provide a better description of the data in the 1600–2000 Å region. Unfortunately, even small differences in (T_{eff}, log g, [Fe/H]) lead to significant variations in the UV fluxes predicted by both classical and T_{min} models, thus making it difficult to identify precisely the proper R for each star. Nevertheless, it is possible to derive the range of acceptable R-values that give predictions in agreement with observations. For each star, we compared observations and T_{min} models by using the combined *IUE-ANS* index $m_{18} - V + m_{15W} - V$, and computed N_{mod} values of R by linear interpolation.

The results are reported in Table 1. A colon (:) indicates that the interpolation was based on $m_{18} - V$ only; for HD 9279, R is missing because of low-quality data in the 15W

and 18 bands. The uncertainty in R arising from the uncertainties in the atmospheric parameters can be evaluated from the spread in the results for stars with $N_{mod} > 1$. The range $\Delta R = R_{max} - R_{min}$ reaches a maximum value of $\Delta R_{max} = 0.07$. In the following discussion, we assume, to be conservative, that ΔR_{max} is also the uncertainty to be assigned to R for the star with $N_{mod} = 1$.

Figure 8 shows, for the 52 stars with computed R, the distribution of the R_{star} values ($R_{star} = R$ for $N_{mod} = 1$, $R_{star} = \langle R \rangle$ for $N_{mod} > 1$). We find $\langle R_{star} \rangle = 0.82$ and $\sigma = 0.04$. The range ΔR_{star}, computed ignoring the outlier at $R_{star} = 0.70$, is 0.13, which is about 2 times ΔR_{max}, thus suggesting an intrinsic dispersion.

The R_{star} values do not show any clear trends either with $B - V$ or with rotational velocity (even if the limited range 5–25 km s^{-1} for the 19 program stars with measured $v \sin i$ does not permit us to derive sound conclusions).

As far as the region shortward of 1600 Å is concerned, the T_{min} models do not provide as good a description of the observations as in the region of 1600–2000 Å, irrespective of
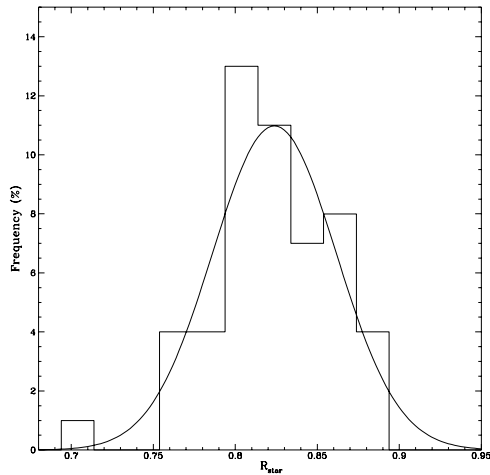
FIG. 8.—Histogram of 52 R_{star} values; the Gaussian with the same mean and standard deviation of the data is superimposed.

the T_{min}/T_{eff} values. It must be noted that in the former region, the *IUE* data are somewhat noisy, in particular shortward of 1500 Å, but the residual fluxes, after descattering, show a plateau, while the T_{min} model fluxes drop significantly. These results suggest an increase in temperature outward in the upper atmospheric layers, and thus the presence of a chromosphere above the temperature minimum region. To investigate this scenario, we studied the case of a "solar analog" star. Our sample includes HD 72905, HD 95128, and HD 186427, which are listed as solar analog stars by Cayrel de Strobel (1996). Unfortunately, as already stated above, the quality of the observations shortward of 1500 Å is not very high. Therefore, we decided to average
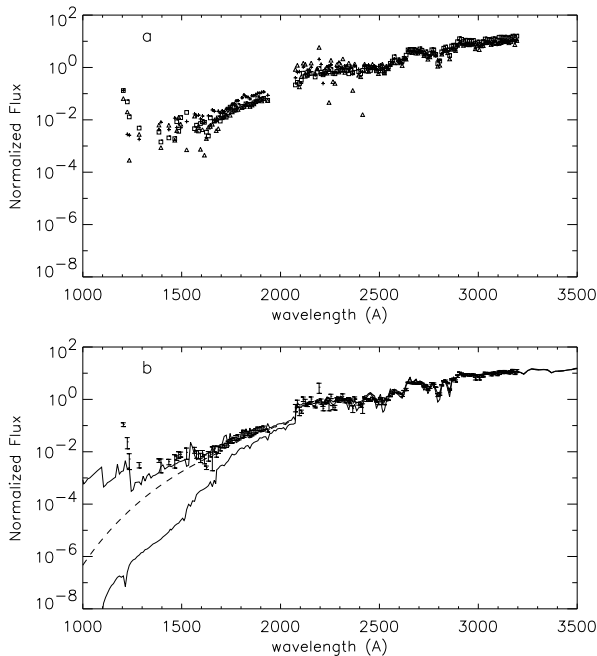

FIG. 9.—(*a*) Normalized flux distribution of HD 72905 (*crosses*), HD 95128 (*triangles*), and HD 186427 (*squares*). (*b*) Average normalized flux distribution (error bars represent the standard deviations of the mean) and synthetic fluxes computed from different models: the R. L. Kurucz (1997, private communication) classical model (*thin line*), the T_{min} model for the Sun with $T_{min}/T_{eff} = 0.81$ (*dashed line*), and a hybrid model (*thick line*).
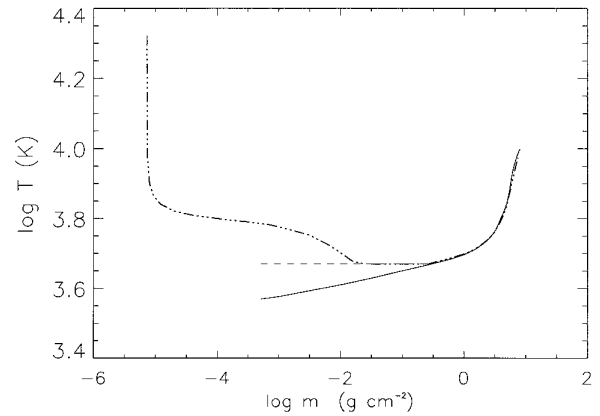

FIG. 10.—Atmospheric structure of different models: R. L. Kurucz (1997, private communication) solar classical model (*solid line*), T_{min} model for the Sun with $T_{min}/T_{eff} = 0.81$ (*dashed line*), and a hybrid solar model (*dash-dotted line*).

the SEDs of the three stars, in order to get a better S/N ratio, and to use the resulting fluxes as representative of a star with the same photospheric parameters as the Sun.

Figure 9*a* shows the relatively good consistency of the three individual SEDs, and Figure 9*b* shows the comparison of the averaged fluxes with the predictions from

1. The classical Kurucz solar model.
2. The T_{min} model, characterized by solar photospheric parameters and $T_{min}/T_{eff} = 0.81$.
3. The hybrid model, obtained by merging the temperature structure, $T(m)$, of model 2 with that of the reference model for the quiet Sun from Maltby et al. (1986). In this model, we can identify three regions (see Fig. 10), where m is the mass column density in g cm^{-2}: (*i*) the inner photosphere ($m > 2.636E - 01$), with a $T(m)$ taken from the classical solar model; (*ii*) the external layers ($m < 2.52E - 02$), with a $T(m)$ taken from the Maltby et al. (1986) model; and (*iii*) a temperature minimum region ($2.52E - 02 \leq m \leq 2.636E - 01$), with $T(m) = 0.81 T_{eff}$.

Figure 9 permits us to derive the following conclusions:

1. Any of the above-mentioned models can be chosen to describe the observed data above 2000 Å, where the classical model predictions cannot be distinguished from others.
2. Models 2 and 3 provide a fairly good description of the averaged fluxes in the 1600–2000 Å region.
3. Model 3, which takes into account the presence of the chromosphere above the T_{min} region, is the only one that mimics the trend of the observations shortward of 1600 Å.

4. CONCLUSIONS

In this paper, we studied the role of the UV continuum for predicting the characteristics of the temperature minimum region in the atmosphere of G-type stars by comparing the observed spectral energy distributions of 53 field G stars with predictions from atmosphere models. While the fluxes computed from R. L. Kurucz (1997, private communication) models describe very well the near-UV region, they fail in the *IUE*/SWP region. On the other hand, the theoretical fluxes computed from the T_{min} models proposed here allow us to obtain good agreement with observations down to 1600 Å, thus confirming that the T_{min} atmospheric region determines the level of the continuum flux in the 1600–2000 Å range.

First-order modeling of the upper photosphere (where nonradiative heating plays a significant role), assuming a constant temperature outward of the temperature minimum layer, even if very crude, works quite effectively, but in the far ultraviolet. The only ad hoc parameter, namely $R = T_{min}/T_{eff}$, could be determined by comparing observed and computed fluxes in the ultraviolet region 1600–2000 Å. The uncertainties in the atmospheric parameters determine a spread on the order of 0.07 on individual R_{star}. The statistical results for our sample are consistent with those from high-resolution analyses of chromospheric emission lines of individual stars. The statistical behavior suggests an intrinsic dispersion in R_{star}, the nature of which deserves further investigation.

The UV continuum shortward of 1600 Å is strongly affected by the presence of the chromosphere; thus, a hybrid structure similar to that of the semiempirical model for the Sun of Maltby et al. (1986) is better suited to describing, for example, the flux of a solar analog star. In the near future, we plan to exploit the possibility of constructing hybrid models for G-type stars by using constraints from high-quality data in the far-UV, such as those provided by GHRS and the forthcoming *Far-Ultraviolet Spectroscopic Explorer*. Nevertheless, we want to stress the fact that the use of more sophisticated models does not affect the results presented in this paper, since the introduction of the chromosphere does not significantly affect the determination of R_{star}.

In conclusion, the presence of the UV excess is ubiquitous in G-type stars, and the UV continuum itself contains a strong signature of the temperature minimum region and chromosphere in their outer atmospheres. Furthermore, the temperature minimum value can be determined by using first-approximation atmosphere models such as those adopted in this paper.

REFERENCES

Basri, G. 1985, NASA *IUE* Newsletter, 28, 58

Basri, G., Clarke, J. T., & Haisch, B. M. 1985, A&A, 161

Cayrel de Strobel, G. 1996, A&A Rev., 7, 243

Cayrel de Strobel, G., Soubiran, C., Friel, E. D., Ralite, N., & François, P. 1997, A&AS, 124, 299 (1996 Catalog)

Edvardsson, B., Andersen, J., Gustafsson, B., Lambert, D. L., Nissen, P. E., & Tomkin, J. 1993, A&A, 275, 101

Gessner, S. E., Carpenter, K. G., & Robinson, R. D. 1994, AJ, 107, 747

Haisch, B. M., & Basri, G. 1985, ApJS, 58, 179

Haisch, B., & Schmitt, J. H. M. M. 1996, PASP, 108, 113

Kelch, W. L., Linsky, J. L., & Worden, S. P. 1979, ApJ, 229, 700

Kjærgaard, P., Nørgaard-Nielsen, H. U., Cacciari, C., & Wamsteker, W. 1984, A&A, 133, 363

Kurucz, R. L. 1993, CD-ROM 13, ATLAS 9 Stellar Atmosphere Programs and 2 km/s Grid (Cambridge: Smithsonian Astrophys. Obs.)

Malagnini, M. L., Morossi, C., & Franchini, M. 1994, in ASP Conf. Ser. 64, Cool Stars, Stellar Systems, and the Sun, ed. J.-P. Caillault (San Francisco: ASP), 584

Maltby, P., Avrett, E. H., Carlsson, M., Kjeldseth-Moe, O., Kurucz, R. L., & Loeser, R. 1986, ApJ, 306, 284

Morossi, C., Franchini, M., & Malagnini, M. L. 1997, in IAU Symp. 189, Fundamental Stellar Properties: the Interaction between Observation and Theory, ed. T. R. Bedding, A. J. Booth, & J. Davis (Dordrecht: Kluwer), 93

Morossi, C., Franchini, M., Malagnini, M. L., Kurucz, R. L., & Buser, R. 1993, A&A, 277, 173

Space Telescope Science Institute. 1995, Space Telescope Science Data Analysis System (Ver. 1.3.4; Baltimore: STScI)

Wesselius, P. R., Van Duinen, R. J., de Jonge, A. R. W., Aalders, J. W. G., Luinge, W., & Wildeman, K. J. 1982, A&AS, 49, 427 (*ANS* Catalog)